

Evolution of Cluster Morphology: X–ray data *vs* CDM models

Riccardo Valdarnini¹, Simona Ghizzardi^{2,3} and Silvio Bonometto^{2,3}

¹*SISSA – International School for Advanced Studies, Via Beirut 2/4, Trieste, Italy*

²*Department of Physics of the University, Via Celoria 16, Milano, Italy*

³*INFN – Sezione di Milano*

Accepted 1997 ** *. Received 1997 ** **; in original form 1997 ** **

ABSTRACT

We compare the evolution of morphology in X–ray cluster data and in clusters obtained in a simulation of flat CDM, normalized to the observed cluster abundance. We find that the evolution rate in model clusters is significantly higher than in data clusters. The results is striking, as our cluster data are all just for $z \lesssim 0.2$, but is not contrary to expectations, as is known that the CDM spectrum is too flat, around the cluster scale, and therefore induces the presence of too many substructures. The cluster simulations were run using a TREESPH code and therefore include hydrodynamical effects. The test we performed, which turns out to be very sensitive, starts from the so-called power ratios introduced by Buote and Tsai, and makes use of the 2–dimensional generalization of the Kolmogorov–Smirnov test. The discrepancy between data and model is however directly visible through linear regression techniques and using simpler statistical tests.

Key words: Galaxies: clusters: general – galaxies: evolution – X–ray: galaxies – cosmology: theory – cosmology: simulations.

1 INTRODUCTION

The principal aim of this work is to study the evolution of morphology in hydrodynamical simulations of galaxy clusters, for flat CDM cosmological models, normalized in order to reproduce the observed cluster abundance. We also compare its trend with observational X–ray data and find a substantial discrepancy on the rate of evolution of substructures, which seem to evolve faster in models than in data.

This result is not surprising, as the slope of CDM spectrum, around the cluster scale, is known to be too flat. E.g., the *extra power* parameter $\Gamma = 7.13 \cdot 10^{-3} (\sigma_8/\sigma_{25})^{10/3}$ ($\sigma_{8,25}$ are mass variances on 8,25 $h^{-1}\text{Mpc}$ scales; $h = H/100 \text{ km s}^{-1}\text{Mpc}^{-1}$) is significantly lower in data than in model predictions: for APM galaxies, Peacock and Dodds (1995) found $\Gamma = 0.23 \pm 0.04$; for the Abell/ACO sample, Borgani et al. (1997) found Γ in the interval 0.18–0.25; on the contrary CDM models predict $\Gamma \simeq 0.4$.

What is however striking is the sensitivity that the

tests we performed on hydrodynamical simulations, seem to have in appreciating the spectral slope. High Γ values imply that too many substructures intervene in the dynamical growth of fluctuations, on cluster scales. An excess evolution can be therefore expected. But available data cover only a narrow redshift interval ($0 < z < 0.2$) and simulation outputs shall be used on the same interval, reproducing data distribution. The point is then that different rates seem already visible on such redshifts, which concern a fairly recent cosmic evolution.

The tests we use start from the a statistical tool introduced by Buote & Tsai (1995), who defined the so-called power ratios $\Pi^{(m)}$, which essentially derive from a multipole expansion of X–ray surface brightness. In sec. 2 more details on $\Pi^{(m)}$ definition will be reported. Much work on $\Pi^{(m)}$ was already done, both in order to derive them from data and to compare them with simulations (Buote & Tsai 1995, Buote & Tsai 1996, Tsai & Buote 1996, Buote & Xu 1997). In a recent work, Buote & Xu (1997) gave some plots where the evolution of cluster morphology in data and CDM simulations are compared; similar plots are given also by us.

Here, however, we present two essential improvements: (i) Instead of using pure CDM N–body simulations, we use the outputs of a TREESPH code, therefore including hydro-

† E-mail: valda@sissa.it;
ghizzardi@mi.infn.it;
bonometto@mi.infn.it

dynamical effects. A large number of massive clusters are treated in this way and hydrodynamical effects are found to be important in shaping the distribution of the X-ray emitting baryon component. This will be shown in some plots where DM and baryon distributions are compared; but there is also a back effect of the different baryon distributions on the evolution of the potential well, which cannot be appreciated directly from the plots. (ii) Furthermore, to compare data and simulations, we use an advanced statistical discriminator (Peacock 1982, Fasano & Franceschini 1987), which allows us to find quantitative estimates of the probability that the same process gives rise to observational and simulated statistical outputs. The discrepancy we find is however directly visible in suitable evolutionary plots and can be also appreciated using a simpler statistical test.

The plan of the paper is as follows. In Sec. 2 power ratios are defined and their evolution is discussed. In Sec. 3 we give some details about the model and simulation procedure followed to define clusters and study their evolution. Power ratios are computed in Sec. 4 where we also perform the comparison between data and simulations. Results are discussed in Sec. 5, where some general conclusions are also drawn. Appendix A includes a brief outline of the PF2 statistical test, and some discussion of the reasons why its extension to three dimensions is premature.

2 POWER RATIOS: DEFINITION AND EVOLUTION

In this section we shall report results of Tsai & Buote (1996) and Buote & Xu (1997), which are the starting point of our arguments. The steps to work out the power ratios from a model cluster are the following ones: (i) We assume that the X-ray emission power is $\propto \rho_b^2(\mathbf{r})$ and project it on a random plane π_r , yielding a surface brightness $\Sigma(x, y)$ (apart of a proportionality factor). (ii) We find the projected mass center (or *centroid*) O for $\Sigma(x, y)$; in respect to O , the surface brightness can be expressed as $\Sigma(R, \varphi)$; (iii) we use such Σ to generate a pseudo-potential $\Phi(R, \varphi)$, by solving the Poisson equation:

$$\nabla^2 \Phi = \Sigma(R, \varphi) \quad (1)$$

(again, a constant factor, in front of the r.h.s. – *e.g.*, the gravitational constant G , – would turn out to be irrelevant). (iv) We expand Φ in multipoles; from the coefficients of such expansion, the power ratios $\Pi^{(m)}(R)$ are obtained. More in detail:

$$\Pi^{(m)}(R) = \log_{10}(P_m/P_0) \quad (2)$$

where

$$P_m(R) = \frac{1}{2m^2}(\alpha_m^2 + \beta_m^2), P_0 = [\alpha_0 \ln(R/\text{kpc})]^2 \quad (3)$$

and

$$\alpha_m = \int_0^1 dx x^{m+1} \int_0^{2\pi} d\varphi [\Sigma(xR, \varphi) R^2] \cos(m\varphi) \quad (4)$$

$$\beta_m = \int_0^1 dx x^{m+1} \int_0^{2\pi} d\varphi [\Sigma(xR, \varphi) R^2] \sin(m\varphi) \quad (5)$$

Henceforth, the constants which were unspecified cancel out, when the ratio of P_m 's is considered. Moreover, owing to the

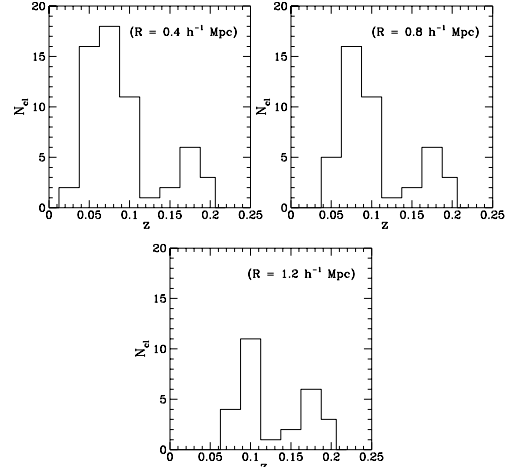


Figure 1. Redshift distribution of data clusters for $R = 0.4, 0.8, 1.2h^{-1}\text{Mpc}$

definition of the centroid O , P_1 vanishes and $\Pi^{(1)}$ should then be disregarded. As we restricted the analysis to $m \leq 4$, which account for substructure scales not much smaller than R itself, there are only 3 significant $\Pi^{(m)}$ ($m = 2, 3, 4$).

Therefore, during its evolution, a cluster moves along a line (*evolutionary track*) in the 3-dimensional space spanned by such $\Pi^{(m)}$'s, whose 2-dimensional projections will be considered below. Starting from a configuration away from the origin, corresponding to a large amount of internal structure, a cluster evolves towards isotropization and homogeneization. This motion, however, does not occur with a steady trend, as sudden bursts of structure appear when further matter lumps approach the cluster potential well, to be absorbed by it. However, the evolutionary track eventually approaches the origin, and this can be more easily appreciated by averaging over the contributions of several clusters.

Actual data, of course, do not show the motion of a single cluster along the evolutionary track. Different clusters, however, lie at different redshifts and, in average, can be expected to describe a succession of evolutionary moments. Power ratios for model clusters are to be set in the 3-dimensional space spanned by $\Pi^{(m)}$'s, taking each model cluster at redshifts distributed as for data clusters.

The data set is the same of Buote & Tsai (1996). Among X-ray cluster images, taken with *ROSAT* PSPC (Pfeffermann et al. 1987), and such that the PSPC central ring contains a cluster portion whose radius exceeds $400 h^{-1}\text{kpc}$, they took those contained in the HEASARC-legacy database and belonging to the Ebeling (1993) or Edge et al. (1990) samples. Out of the 59 objects selected in this way, they could estimate $\Pi^{(m)}$ for 44 of them at $R = 0.8 h^{-1}\text{Mpc}$ and for 27 of them at $R = 1.2 h^{-1}\text{Mpc}$. PSPC data give the X-ray surface brightness $\Sigma_X(R, \varphi)$, which is to be used in the same way as the Σ 's obtained from models, to work out $\Pi^{(m)}$ for $R = 0.4, 0.8, 1.2 h^{-1}\text{Mpc}$.

In fig. 1 we give the redshift distribution of data clusters, for the three values of R . As we shall discuss further in the next section, we have 40 simulated clusters to deal with. We take each of them, only at a single z value, producing 50

z distributions similar to real data. In order to work out power ratios, we need to treat each cluster with reference to a given plane: 50 random planes are selected for each cluster and one of them is considered for each z sequence.

3 THE SIMULATIONS

The main contribution of this work is given by the simulations we run, to work out $\Pi^{(m)}$, and that will be however used for several other aims. We started from a box with a side $L = 200 h^{-1} \text{Mpc}$, where we evolved a CDM model with $h = 0.5$ and $\Omega_b = 0.06$. The initial spectrum was normalized in order that the cumulative cluster number density $n(> M)$, for $M = 4.2 h^{-1} 10^{14} M_\odot$, yields $N_{cl} = n(> M)L^3 = 32$, according to data on cluster abundance (White et al. 1993, Biviano et al. 1993, Eke et al. 1996). This corresponds to $\sigma_8 = 0.52$. The simulation was run from $z_{in} = 6.3$ to $z = 0$ using a P3M code with 10^6 particles (mass $m_p = 1.78 \cdot 10^{13} M_\odot$). The choice of such z_{in} value is dictated by the opportunity of restarting from the same conditions when hydrodynamic simulations are then performed. The PM part of the code makes use of 256^3 cells and a smoothing radius of 520 kpc was taken for gravitational forces.

At $z = 0$ clusters were then identified using a FoF algorithm; we considered as *friends*, particles at a distance $< 0.2\lambda$ (λ is the mean particle separation). The 40 most massive clusters were then located; the lightest one is made by 34 particles and has a mass $M_m \simeq 6 \cdot 10^{14} M_\odot$.

For each of these clusters an hydrodynamic simulation was then performed, using a TREESPH code. The hydrodynamical part of the code is based on the SPH method (Hernquist & Katz 1989). The gravitational forces are solved with a hierarchical tree algorithm and this part of the code is based on the public treecode of L. Hernquist (Hernquist 1987). In order to run the hydrodynamical simulation we located the cluster center at $z = 0$ and found all particles within a radius r_{200} , where the cluster density is $\simeq 200 \langle \rho \rangle$ (background density). Such particles were traced back to z_{in} , in the original simulation cube, and a smaller cube of side L_c , enclosing all of them, was then located at the cluster center. We found the approximate scaling $L_c \simeq 45 \text{Mpc} \times (r_{200}/3.43 \text{Mpc})$.

A high resolution lattice of 22^3 particles was set in the smaller cube and their position was then perturbed, using the same initial conditions of the cosmological simulations, implemented by additional waves to sample the increased Nyquist frequency. This technique is similar to the one adopted by Katz & White (1993), Navarro, Frenk & White (1995). We used two grids, for baryon and CDM particles, whose masses $m_b/m_{CDM} = \Omega_b/(1 - \Omega_b)$.

The cube of side L_c is then set inside a greater cube of side $2L_c$, with parallel sides and equal center. Such greater cube is initially filled by 22^3 CDM particles, whose spacing is double in respect of inner cube particles, and whose mass is $8m_{CDM}(1 + \Omega_b)$. Then particles falling in the smaller inner cube are eliminated. Heavier particle positions are also perturbed, according to the initial conditions of the cosmological simulation. Finally, we use all particles inside a sphere, of radius L_c and with the same center as cubes, for the high resolution TREESPH simulation.

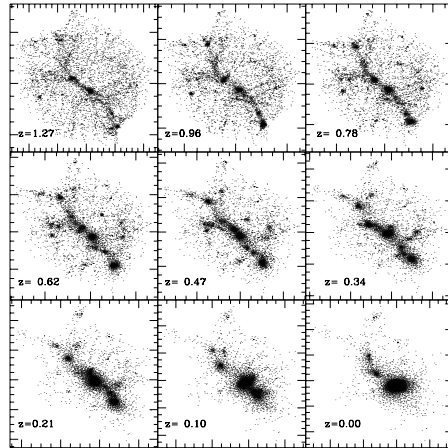


Figure 2. Density projections of a simulated cluster at several redshift.

Since we take a constant number of grid particles, their masses vary according to L_c ; for the most massive cluster we met ($M_{200} \simeq 10^{15} M_\odot$), it was $m_{gas} = 3.4 \cdot 10^{10} M_\odot$. The softening parameter for gravitational forces (ε) was set to $\varepsilon_g = 80 \text{kpc}$ for gas particles and scales as $\propto m^{1/3}$. We use a tolerance parameter $\theta = 0.7$, without quadrupole corrections. Viscosity was set as in Hernquist & Katz (1989) taking their parameters $\alpha = 1$ and $\beta = 2$.

The minimum timestep was $3 \cdot 10^6 \text{yr}$ for gas particles and twice as much for CDM. In average each cluster required ~ 6 hours of CPU time to be evolved from z_{in} to $z = 0$ on a RISK 6000 elaborator. Outputs from TREESPH simulations were preserved at various redshifts. Among the smaller ones, we used $z_i = 0.15, 0.10, 0.049$ and 0 ($i = 1, \dots, 4$).

In fig. 2 we give a typical example of projected ρ_b outputs, at a set of redshifts ≤ 1.27 . Already from such figure, it is clear that CDM clusters are rich of substructures and characterized by a fast substructure evolution. In fig. 3 we show CDM and baryon distributions at $z = 0$ for a typical cluster. Such figure shows that the baryon distribution is significantly smoothed out in respect to CDM. This obviously reflect on $\Pi^{(m)}$'s, although we shall report no quantitative details on this point here.

4 CLUSTER EVOLUTION FROM POWER RATIOS BEHAVIOUR

Clusters are expected to evolve by accreting lumps of baryons and CDM onto a deep potential well. As time elapses, nearby lumps are gradually absorbed and cluster substructures tend to vanish. Such behaviour is clearly visible also in fig. 2. In fig. 4, instead, we give 9 plots for the space containing the evolutionary tracks projected on 3 planes and at three different R 's. Cross indicate the location of data clusters. Filled dots refer to a single selection of simulated clusters. The trend visible in this selection of simulated clusters is however a general feature: a linear regression gives place to the dotted straight line reported in the plots. Although real data do not show such a marked

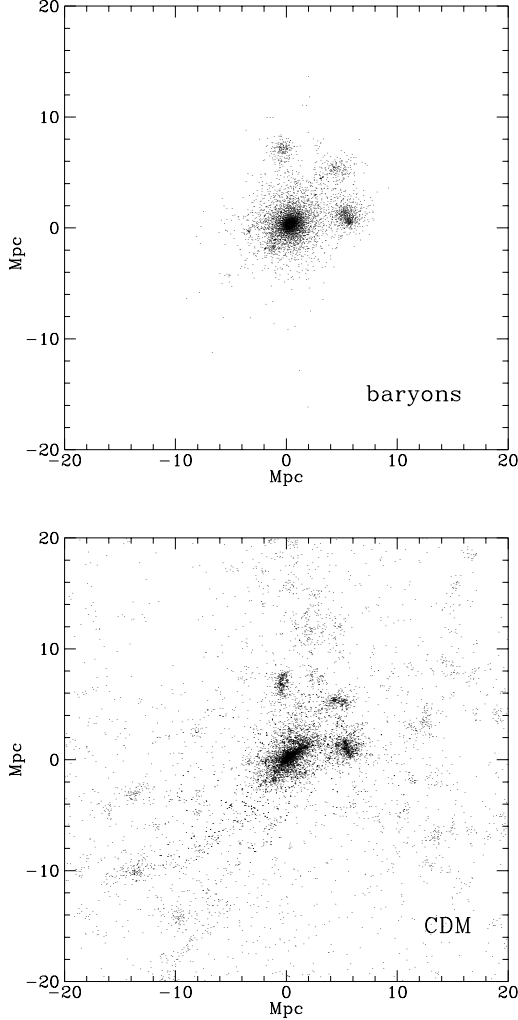


Figure 3. *Baryon and dark matter density projections of a simulated cluster*

trend, a linear regression was performed also on them. The continuous lines show the results of such linear fits to data.

Fig. 4 shows that model lines are steeper than data lines *in all cases*. This behaviour is true for all model sets we explored and indicates a faster evolution of model clusters in respect to the real ones. In Table 1, we report the values of the angular coefficients m of the two straight lines of each plot, together with 1σ errors Δm , obtained from the linear regression.

Another way of testing the stability of m amounts to performing a bootstrap-resampling of the simulation points. In fact, the 2-dimensional point distributions are rather irregular and a bootstrap approach tests the reliability of the linearity assumption, together with the actual m values.

Bootstrap resampling was performed selecting clusters with the correct z distribution, but allowing data repetition. All resamplings confirmed that model fits are steeper than data. Furthermore, bootstrap errors are systematically smaller than errors from linear regressions. Average errors from 20 bootstrap resamplings are reported in parenthesis in Table 1, aside of those from linear fits.

Table 1. Angular coefficients and standard deviations for linear fits. Indexes d s refers to data and simulations. In parenthesis we give also simulation errors from 20 bootstrap resamplings.

Rh/Mpc		m_d	Δm_d	m_s	Δm_s
0.4	Π_2 vs. Π_3	0.29	0.19	0.64	0.18 (0.036)
	Π_2 vs. Π_4	0.52	0.14	0.85	0.12 (0.026)
	Π_3 vs. Π_4	0.38	0.10	0.61	0.11 (0.011)
0.8	Π_2 vs. Π_3	0.51	0.15	0.87	0.15 (0.020)
	Π_2 vs. Π_4	0.91	0.14	1.03	0.12 (0.010)
	Π_3 vs. Π_4	0.71	0.14	0.92	0.07 (0.004)
1.2	Π_2 vs. Π_3	0.43	0.16	0.87	0.10 (0.008)
	Π_2 vs. Π_4	0.18	0.20	0.97	0.11 (0.008)
	Π_3 vs. Π_4	0.51	0.21	1.03	0.07 (0.009)

Table 2. Kolmogorov–Smirnov test on angular coefficients for the sequence yielding fig. 4 and averaged on 50 redshifts sets.

Rh/Mpc		KS-test	KS-test (av.)
0.4	Π_2 vs. Π_3	1.61E-22	3.21E-23
	Π_2 vs. Π_4	6.43E-32	1.29E-32
	Π_3 vs. Π_4	3.79E-29	7.60E-30
0.8	Π_2 vs. Π_3	1.48E-22	1.62E-08
	Π_2 vs. Π_4	5.75E-05	0.12E+00
	Π_3 vs. Π_4	1.72E-19	1.65E-16
1.2	Π_2 vs. Π_3	1.19E-20	3.41E-16
	Π_2 vs. Π_4	6.52E-24	6.24E-24
	Π_3 vs. Π_4	4.45E-22	1.07E-18

In Table 2 we report the the results of a Kolmogorov–Smirnov test applied to the line slopes of the single case considered in Fig. 4, and the values obtained by averaging on the set of 50 realizations. The figures are the probabilities that the different slopes we find in data and models can be due to the same process, taking into account the number of data points in use. This test reproduces the visual feeling that the two straight lines, coming from data and simulations, have a systematically different slope. (Using bootstrap errors as Δm , besides of being scarcely significant, would lead to even smaller probabilities.) This test, however, is somehow misleading and actual probabilities are substantially greater than so. The extra input that we should eliminate, to obtain the probability that the observational data set is fit by artificial data sets, is the requirement of linear behaviour. This can be done by applying the generalization of the Kolmogorov–Smirnov test to 2-dimensional data sets, proposed by Peacock (1982) and widely tested by Fasano & Franceschini (1989). We shall refer to this estimate as PF2 test and more details on it will be given in Appendix A. In Table 3 we give the values of the single case of Fig. 4 and the averaged values of the PF2-probabilities that the observational data set and each artificial data set are realizations of the same process, for each Π_m pair and each R value. Such average PF2-probabilities are not so small as those reported in Table 2 and essentially correspond to a

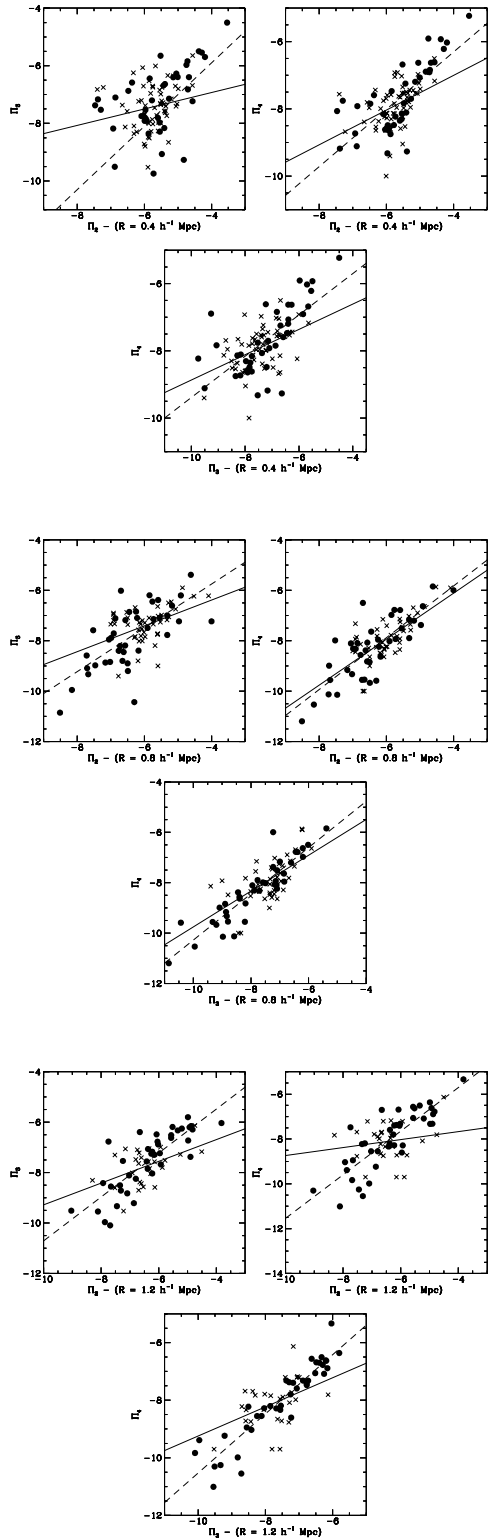


Figure 4. Power ratios and evolutionary tracks for data and simulated clusters at three aperture radii. Crosses and continuous lines refer to the observational sample, filled dots and dashed lines refer to one of the artificial sequences of 40 clusters, with similar z distribution. Plots obtained from all 50 cluster sequences are strictly analogous.

Table 3. PF2- test on Π_m for the sequence yielding fig. 4 and averaged on 50 redshifts sets.

$R h/\text{Mpc}$		PF2-test	PF2-test (av.)
0.4	Π_2 vs. Π_3	0.129	0.057
	Π_2 vs. Π_4	0.045	0.052
	Π_3 vs. Π_4	0.073	0.079
0.8	Π_2 vs. Π_3	0.017	0.076
	Π_2 vs. Π_4	0.038	0.087
	Π_3 vs. Π_4	0.031	0.052
1.2	Π_2 vs. Π_3	0.038	0.053
	Π_2 vs. Π_4	0.050	0.034
	Π_3 vs. Π_4	0.016	0.054

$\sim 2\sigma$ discrepancy. However, even this sophisticated test is unable to work out a final value which takes into account all the above partial results. There can be however little doubt left that such a sequence of values, where a faster evolution in model in respect to data is systematic, could hardly be due to observational sample biases or to disregarding peculiar physical effects in the simulations, and is more likely to indicate that the model is not adept to reproduce real data.

5 CONCLUSIONS

It has been known for several years that COBE normalized CDM yields a cluster abundance exceeding observation by a factor ~ 20 . In order to obtain a fair number of clusters, the quadrupole data has to be lowered down to $\sim 9 \mu\text{K}$, at more than 3σ 's from the observational value. However, CDM models are still currently in use as reference models; in fact, Λ CDM models, mixed models or Λ models, used to obtain fair fits of observational data on various scales, involve more parameters.

According to our results, however, even though CDM is normalized to yield a fair number of clusters, we cannot expect their morphologies to be adequately approached by the model. This output is related to the slope of the transferred spectrum, as already outlined in Sec. 1, and as is expressed by the values of the *extra power* parameter Γ . It is however important and fairly unexpected that the effects of such different slope are already visible in the average evolutionary tracks, for a fairly narrow redshift range ($0 < z < 0.2$) as the one we had in observational data.

In a forthcoming paper, based on work in progress, we shall extend this analysis to other cosmological models, whose transferred spectrum has a Γ value consistent with observations. This is important, in order to test how sensitive the power ratios Π_m are to the Γ value and to check whether this test depends only on Γ or, *e.g.*, also on the *substance* of the model considered.

ACKNOWLEDGMENTS

It is a pleasure to thank David Buote for his useful comments. One of us (S.G.) wishes to thank SISSA for its hospitality during the preparation of this work.

REFERENCES

- Biviano A., Girardi M., Giuruciu G., Mardirossian F., Mezzetti M. 1993 *ApJ*, 411, L13
- Borgani S., Moscardini L., Plionis M., Górski K.M., Holzman J., Klypin A., Primack J.R., Smith C.C., Strompor R., 1997, *New Astr.* 321,1
- Buote D.A., 1997, preprint astro-ph 9705221, *MNRAS* (in press)
- Buote D.A., Tsai J.C., 1995, *ApJ*, 452, 522
- Buote D.A., Tsai J.C., 1996, *ApJ*, 458, 27
- Buote D.A., Xu G., 1997, *MNRAS*, 284, 439
- Ebeling H., 1993, *Ph.D Thesis, Ludwig-Maximilians-Univ. Munchen*
- Edge A.C., Stewart G.C., Fabian A.C., Arnaud K.A., 1990 *MNRAS*, 245, 559
- Eke V.R., Cole S., Frenk C.S., 1996 *MNRAS* 282, 263
- Fasano G., Franceschini A., 1987, *MNRAS*, 225, 155
- Hernquist L. 1987, *ApJS*, 64, 715
- Hernquist L., Katz N., 1989, *ApJS*, 70, 419
- Katz N., White S.D.M., 1993, *ApJ*, 412, 455
- Navarro J., Frenk C.S., White, S.D.M., 1995, *MNRAS*, 275, 720
- Peacock J.A., 1983, *MNRAS*, 202, 615
- Peacock J.A., Dodds S.J., 1994, *MNRAS*, 267, 1020
- Pfeffermann E. et al., 1987, *Proc. SPIE*, 733, 519
- Press W.H., Teukolsky S.A., Vetterling W.T., Flannery B.P., 1992, *Numerical Recipes, Cambridge University Press*
- Tsai J.C., Buote D.A., 1996, *MNRAS*, 282, 77
- White S.D.M., Efstathiou G., Frenk C.S., 1993, *MNRAS* 262, 1023

APPENDIX A – The PF2 test

As is known, the Kolmogorov–Smirnov (KS) test is used to evaluate the probability that 2 distributions on a single variable x are produced by the same process. If N events are located at x_i ($i = 1, \dots, N$), let $S_N(x)$ give the fraction of events located at $x_i < x$. Clearly S_N is discontinuous in each x_i , where it increases by $1/N$. Let two sets of N_1 and N_2 events yield S_{N_1} and S_{N_2} ; the KS statistics is then defined as the maximum distance between them:

$$D = \max_{\{any\ x\}} |S_{N_1}(x) - S_{N_2}(x)| \quad (a1)$$

and it can be shown that the probability that the two data sets are produced by the same process can be estimated, by using D , as follows: Let be

$$1/\nu^2 = 1/N_1 + 1/N_2 \quad (a2)$$

and $u = D(\nu + 0.12 + 0.11/\nu)$. Then such probability reads:

$$KS(u) = 2 \sum_{r=1}^{\infty} [(-1)^r / \exp(2r^2 u^2)] . \quad (a3)$$

Various numerical routines exist which allow to evaluate such function with any desired approximation (see, *e.g.*, Press et al. 1992).

While for one-dimensional distributions the meaning and the building of D are simple (it tells us the maximum difference of integrated distributions), in the case of two-dimensional distributions the events are not ordered and there is no immediate way of telling where such difference is maximum. A further problem is set by the degree of correlation amongst data. A limiting situation occurs if they locate along a straight line on a plane, and then the KS test would be suitable again.

The problem was considered in detail by Peacock (1982) and Fasano & Franceschini (1987), whose approach (PF2) we shall briefly report here. If N data are located on the 2-dimensional plane x, y and have average \bar{x}, \bar{y} , let us first define $\xi_i = x_i - \bar{x}$ and $\eta_i = y_i - \bar{y}$. Their correlation coefficient is then:

$$r = (\sum_i \xi_i \eta_i) / (\sqrt{\sum_i \xi_i^2} \sqrt{\sum_i \eta_i^2}) \quad (a4)$$

(notice that, for $r = 1$, the points would actually lie on a straight line). Then, if we have two sets of N_1 and N_2 data, with correlation coefficients r_1 and r_2 , defined according to eq. (a4), we define

$$\tilde{r} = \frac{1}{2} \sqrt{r_1^2 + r_2^2} \quad (a5)$$

as square average correlation.

The basic point, however, amounts to define a 4-value extension of the function S_N , for each set of N data: the 4 values are the fractions of data in each of the four *quadrants* set by the point x, y where S_N is evaluated. The PF2 statistics D will be the maximum difference between S_{N_1} and S_{N_2} values, ranging both over points and quadrants. Using such D , the square average correlation r , and ν , defined according to eq. (a2), we then define

$$u = \nu^2 D / [\nu + \sqrt{1 - \tilde{r}^2} (0.25\nu - 0.75)] \quad (a6)$$

and, using eq. (a3), we obtain the required probability.

It ought to be outlined that there are some restrictions to the significance of these probability estimators. In general, they become safer as ν increases. However, in the one-dimensional case, the estimate is good for $\nu \gtrsim 10-20$ (corresponding to $N_1 \sim N_2 \sim 8$). In the two-dimensional case, the restriction is already much stronger, as it must be $\nu \gtrsim 100-400$ (corresponding to $N_1 \sim N_2 \sim 25$), and the further condition that the probability found is $\lesssim 20\%$ is to be added.

Our sets of data and simulation points are therefore just adequate to meet the above conditions. This is important also in view of a step forward that could be considered: treating directly the 3-dimensional distributions in the parameter space spanned by $\Pi^{(m)}$ ($m = 2, 3, 4$), instead of their two-dimensional projections. An algorithm extending the above test to 3-dimensions is a straightforward generalization; the range of validity of such algorithm, instead, should be accurately tested. A large portion of the work of Fasano and Franceschini (1987) amounted to perform such checks, for the two-dimensional case. However, the trend found between 1 and 2 dimensions, seems to indicate that, in three dimensions, we need 2 sets of data containing $\sim 10^2$ points. As far as simulations are concerned, this requires just doubling our simulation set. Data clusters, instead, are significantly below such limit.

This paper has been produced using the Royal Astronomical Society/Blackwell Science \LaTeX style file.